Efficient dynamic bipedal walking using effects of semicircular feet

Fumihiko Asano†* and Zhi-Wei Luo‡

†*School of Information Science, Japan Advanced Institute of Science and Technology, Ishikawa 923-1292, Japan*
‡*Department of Computer Science and Systems Engineering, Graduate School of Engineering, Kobe University, Kobe 657-8501, Japan*

SUMMARY

Achieving energy-efficient and high-speed dynamic walking has become one of the main subjects of research in the area of robotic biped locomotion, and passive dynamic walking has attracted a great deal of attention as a solution to this. It is empirically known that the convex curve of the foot, which characterizes passive–dynamic walkers, has an important effect on increasing the walking speed.

This paper mainly discusses our investigations into the driving mechanism for compass-like biped robots and the rolling effect of semicircular feet. We first analyze the mechanism for a planar fully actuated compass-like biped model to clarify the importance of ankle-joint torque by introducing a generalized virtual-gravity concept. A planar underactuated biped model with semicircular feet is then introduced and we demonstrate that virtual passive dynamic walking only by hip-joint torque can be accomplished based on the rolling effect. We then compare the rolling effect with a flat feet model through linear approximation, and show that the rolling effect is equivalent to virtual ankle-joint torque. Throughout this paper, we provide novel insights into how zero-moment-point-free robots can generate a dynamic bipedal gait.

KEYWORDS: Dynamic bipedal walking; Semicircular feet; Gait generation; Efficiency, Mechanical energy.

1. Introduction

Passive dynamic walking (PDW)[1] has been considered to provide clues to elucidate the mechanism responsible for energy-efficient dynamic walking. By imitating or modifying the PDW mechanism, several energy-efficient dynamic bipedal walking robots have been achieved thus far.[3–5] Major PDW-inspired approaches to biped-robot control have tended to actuate simple-legged machines gently with small motors, and have successfully achieved efficient biped locomotion. Convex curved feet, on the other hand, have also characterized passive–dynamic walkers,[1] but this has not been a feature of recent biped humanoid robots whose control has been based on the zero moment point (ZMP).[2] The importance of foot shape or the rolling effect has

been empirically recognized;[5,6] however, no theoretical investigations had been done until now.

This paper discusses our studies on the rolling effect of semicircular feet on dynamic bipedal walking based on this observation using theoretical investigation and numerical analysis. Semicircular feet have, as Tedrake *et al.*[6] and Wisse *et al.*[7] pointed out, some valuable effects on legged locomotion; they increase the stable domain and the efficiency of generated gait. In this paper, however, we mainly investigated the rolling effect during the stance phase. We considered the mechanism from the viewpoint of a generalized virtual-gravity concept and clarified how the rolling effect accelerates the robot's center of mass (CoM) during the stance phase.

We first introduce a fully actuated compass-like biped robot with flat feet and analyze the relation between its CoM and joint torques based on inverse transformation and the generalized virtual-gravity concept. The importance of the ankle-joint torque is clarified. Second, an underactuated compass-like biped robot with semicircular feet and underactuated virtual passive dynamic walking (VPDW) only by hip-joint torque are introduced. It is then clarified that the dynamics of the semicircular-feet model can be transformed to that of a fully actuated model with flat feet and the rolling-effect functions as ankle-joint torque through the linearization of the two walking systems and their comparisons. It is theoretically shown that the rolling effect accelerates the robot's CoM forward as virtual ankle-joint torque together with the real hip-joint torque during the stance phase. This paper provides novel insights on biped walking control in *ZMP-free robots* throughout this paper.

The remainder of the paper is organized as follows. In Section 2, a planar fully actuated biped model is introduced and its driving mechanism is analyzed. In Section 3, it is investigate how the joint torques drive the robot's CoM via VPDW. Throughout these two sections, we clarify why the ankle-joint torque is important for efficient walking. In Section 4, a planar underactuated biped model with semicircular feet is introduced, and underactuated virtual passive dynamic walking (UVPDW) is applied to its level gait generation. In Section 5, the rolling effects of semicircular feet as ankle-joint torque is clarified via comparison with a flat-feet model. Also in this section, the effect of semicircular feet on heel-strike collision is discussed. In the subsequent

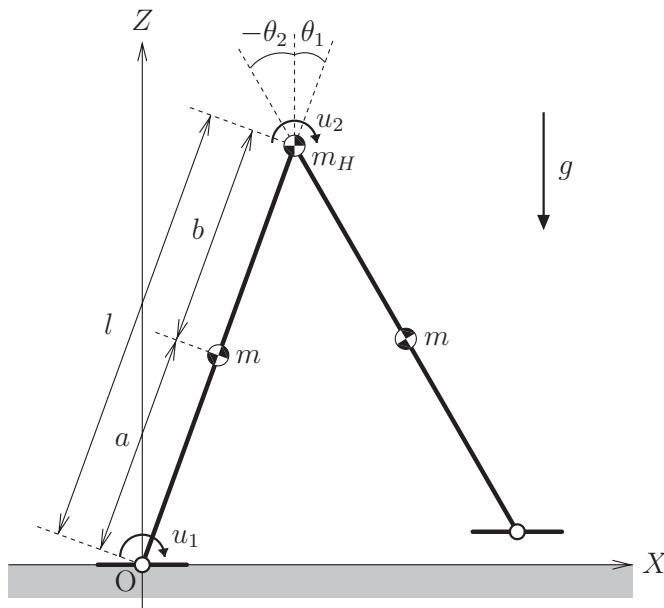* Corresponding author. E-mail: fasano@jaist.ac.jp

Fig. 1. Model of planar fully actuated compass-like biped robot with flat feet.

sections, efficiency of the obtained gait is numerically analyzed in detail. Finally, Section 8 concludes the paper.

2. Model and Mechanism for Planar Fully actuated Compass-like Biped Robot

This paper first presents a planar fully actuated compass-like biped robot as shown in Fig. 1. The details of a biped model are described and the relation between CoM and joint torque is investigated.

2.1. Mathematical model

This subsection describes the mathematical model for a planar fully actuated compass-like biped robot as shown in Fig. 1, which consists of two leg links and three point masses and has flat feet whose mass and thickness can be neglected. The dynamic equation is given by

$$\boldsymbol{M}(\boldsymbol{\theta})\ddot{\boldsymbol{\theta}} + \boldsymbol{C}(\boldsymbol{\theta}, \dot{\boldsymbol{\theta}})\dot{\boldsymbol{\theta}} + \boldsymbol{g}(\boldsymbol{\theta}) = \boldsymbol{Su} = \begin{bmatrix} 1 & 1 \\ 0 & -1 \end{bmatrix} \begin{bmatrix} u_1 \\ u_2 \end{bmatrix}, \quad (1)$$

where $\boldsymbol{\theta} = [\,\theta_1 \ \theta_2\,]^{\mathrm{T}}$ is the generalized coordinate vector, $\boldsymbol{Su}$ is the control input; u_1 is the ankle-joint torque and u_2 is that for the hip-joint. We assumed that the stance foot would always be in contact with the ground without slipping and would have sufficient length according to the ZMP range.

If we assume inelastic collisions for the stance-leg exchange and set suitable values for the physical parameters, the robot can exhibit passive dynamic walking on a gentle slope. In the following, we assumed that the heel-strike collision is perfectly inelastic.

The total mechanical energy of the robot, E [J], is determined as the sum of kinetic and potential energy and

given by

$$E(\boldsymbol{\theta}, \dot{\boldsymbol{\theta}}) = \frac{1}{2}\dot{\boldsymbol{\theta}}^{\mathrm{T}}\boldsymbol{M}(\boldsymbol{\theta})\dot{\boldsymbol{\theta}} + P(\boldsymbol{\theta}). \quad (2)$$

Its time derivative satisfies the relation

$$\dot{E} = \dot{\boldsymbol{\theta}}^{\mathrm{T}}\boldsymbol{Su}. \quad (3)$$

2.2. Relation between center of mass and joint torques

Let $\boldsymbol{r}_g = [\,X_g \ Z_g\,]^{\mathrm{T}}$ be the positional vector of CoM, and its time derivative yields $\dot{\boldsymbol{r}}_g = \boldsymbol{J}_g(\boldsymbol{\theta})\dot{\boldsymbol{\theta}}$, where $\boldsymbol{J}_g(\boldsymbol{\theta}) \in \mathbb{R}^{2\times2}$ is the corresponding Jacobian matrix detailed as

$$\boldsymbol{J}_g(\boldsymbol{\theta}) = M^{-1} \begin{bmatrix} (m_H l + ma + ml)\cos\theta_1 & -mb\cos\theta_2 \\ -(m_H l + ma + ml)\sin\theta_1 & mb\sin\theta_2 \end{bmatrix}$$

$$= \begin{bmatrix} \boldsymbol{J}_X(\boldsymbol{\theta}) \\ \boldsymbol{J}_Z(\boldsymbol{\theta}) \end{bmatrix}, \quad (4)$$

where $M := m_H + 2m$ [kg] is the robot's total mass. $\boldsymbol{J}_g(\boldsymbol{\theta})$ has singularity at $\theta_1 = \theta_2$, and except for this condition, the following inverse transformation from joint torques to the translation force at the CoM is possible.

$$\boldsymbol{f}_g = \boldsymbol{J}_g(\boldsymbol{\theta})^{-\mathrm{T}}\boldsymbol{Su} \quad (5)$$

We call the translation force, $\boldsymbol{f}_g \in \mathbb{R}^2$, *generalized virtual gravity*, which represents a two-dimensional driving force being exerted at the robot's CoM. Equation (5) can be rearranged as

$$\boldsymbol{f}_g = \boldsymbol{J}_g(\boldsymbol{\theta})^{-\mathrm{T}} \left(\begin{bmatrix} 1 \\ 0 \end{bmatrix} u_1 + \begin{bmatrix} 1 \\ -1 \end{bmatrix} u_2 \right)$$

$$= \frac{mbu_1}{M\Delta_g} \begin{bmatrix} \sin\theta_2 \\ \cos\theta_2 \end{bmatrix} - \frac{r_g u_2}{\Delta_g}\frac{\boldsymbol{r}_g}{r_g} =: \boldsymbol{f}_1 + \boldsymbol{f}_2, \quad (6)$$

where $r_g := |\boldsymbol{r}_g|$, $M := m_H + 2m$ is the robot's total mass and

$$\Delta_g := \det(\boldsymbol{J}_g) = -\frac{mb(m_H l + ma + ml)\sin\theta_H}{M^2}, \quad (7)$$

where $\theta_H := \theta_1 - \theta_2$ is the relative hip-joint angle. Note that Eq. (6) is written in the form of two unit vectors. Equation (6) shows that the effect of ankle-joint torque, $\boldsymbol{f}_1$, yields parallel to the swing leg and the effect of hip-joint torque, $\boldsymbol{f}_2$, yields central force, as shown in Fig. 2. Since $\boldsymbol{f}_g$ has singularity at $\theta_1 = \theta_2$, both vectors $\boldsymbol{f}_1$ and $\boldsymbol{f}_2$ diverge at this point and it is ineffective to examine the effect of torque distribution based on this approach. The ratio of $|\boldsymbol{f}_1|$ to $|\boldsymbol{f}_2|$, however, remains finite regardless of singularity as long as u_2 is not zero, which yields

$$\frac{|\boldsymbol{f}_1|}{|\boldsymbol{f}_2|} = \frac{mbu_1}{Mr_g u_2}. \quad (8)$$
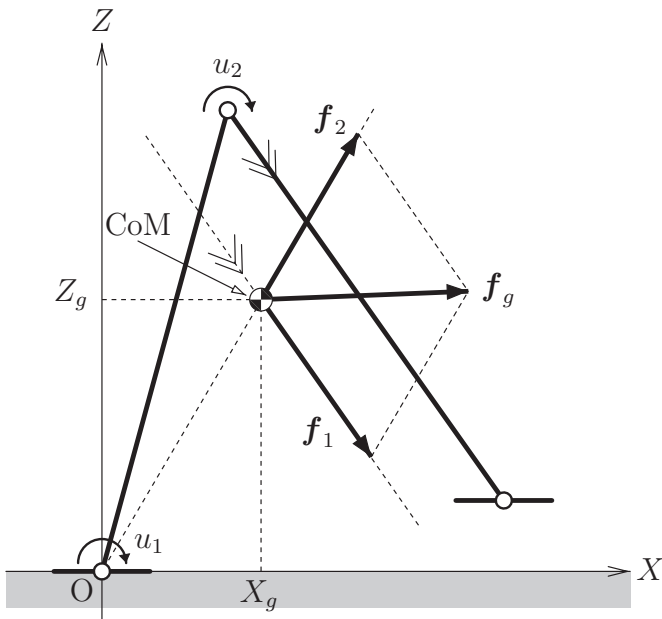
Fig. 2. Relations between generalized virtual gravity vectors at CoM and joint torques.

Table I. Physical parameters of robot.

m_H	10.0 kg
m	5.0 kg
$l = a + b$	1.0 m
a	0.5 m
b	0.5 m

We propose an approach based on the orthogonal projection of $\boldsymbol{f}_i$ on $\dot{\boldsymbol{r}}_g$ in the next section to avoid singularity.

3. Analysis of Virtual Passive Dynamic Walking

We clarified that ankle-joint torque is relatively important and effective in driving a robot's CoM forward. This section then investigates the mechanism responsible for the effect of joint torque and clarifies the importance of ankle-joint torque more deeply from the generalized virtual-gravity point of view.

3.1. Virtual passive dynamic walking

Let i be the link number $(1, 2, \ldots)$ or the hip position (H) in the following, and their corresponding X-positions at each link's CoM are denoted as X_i. The time derivative of X_i is further denoted as $\dot{X}_i = \boldsymbol{J}_{X_i}(\boldsymbol{\theta})\dot{\boldsymbol{\theta}}$, where $\boldsymbol{J}_{X_i}(\boldsymbol{\theta}) \in \mathbb{R}^{1 \times 2}$ is the Jacobian matrix corresponding to X_i. If we assume uniform virtual gravity whose magnitude is $g \tan \phi$ in the X-direction, where ϕ [rad] represents the angle of the virtual slope,[4] the equivalent transformed torque for the total effect of virtual gravity, $\boldsymbol{Su}_{\text{vg}}$, can be expressed as

We now consider the reason why ankle-joint torque is more important than hip-joint torque to drive the CoM forward. In order to prove this question, let us consider the following condition:

$$\frac{|\boldsymbol{f}_1|}{|\boldsymbol{f}_2|} = \frac{mb|u_1|}{Mr_g|u_2|} = 1, \tag{9}$$

which means that the effect of ankle-joint torque, $\boldsymbol{f}_1$, is the same as that of hip-joint torque. The torque ratio is then arranged as

$$\boldsymbol{Su}_{\text{vg}} = \sum_i m_i g \tan \phi \, \boldsymbol{J}_{X_i}(\boldsymbol{\theta})^{\text{T}}, \tag{12}$$

and the time derivative of E is then derived as

$$\frac{|u_1|}{|u_2|} = \frac{Mr_g}{mb} = (mb)^{-1}((m_H l + ma + ml)^2 + m^2 b^2$$

$$-2mb(m_H l + ma + ml) \cos \theta_H)^{1/2}$$

$$\geq \frac{m_H l + 2ma}{mb} = \frac{Ml}{mb} - 2. \tag{10}$$

Note that the value of Eq. (10) is positive because of $M \geq 2m$ and $l \geq b$. The equality in Eq. (10) holds when $\theta_H = 0$. In the case with physical parameters of Table I, for example, the torque ratio yields

$$\frac{|u_1|}{|u_2|} \geq \frac{20.0 \times 1.0}{5.0 \times 0.5} - 2.0 = 6.0, \tag{11}$$

thus u_1 is required at least six times of u_2. For this reason, magnitude of u_1 is much more required to generate the same forward-propelling effect as that of u_2. In other words, u_2 is more sensitive to $\boldsymbol{f}_g$ than u_1 in the meaning of vector norm. In this sense, u_2 seems to be more advantageous than u_1 for propelling the CoM forward; however, excessive use of u_2 increases gravity during the first half of the cycle and disrupts overcoming the potential barrier at mid-stance.

$$\dot{E} = \dot{\boldsymbol{\theta}}^{\text{T}} \boldsymbol{Su}_{\text{vg}} = g \tan \phi \sum_i m_i \dot{\boldsymbol{\theta}}^{\text{T}} \boldsymbol{J}_{X_i}(\boldsymbol{\theta})^{\text{T}} = g \tan \phi \sum_i m_i \dot{X}_i$$

$$= Mg \tan \phi \frac{\text{d}}{\text{d}t} \sum_i \frac{m_i X_i}{M} = Mg \tan \phi \dot{X}_g. \tag{13}$$

This leads to the following:

$$\frac{\partial E}{\partial X_g} = Mg \tan \phi, \tag{14}$$

which is a unified property of passive dynamic walking. Following Eqs. (3) and (13), we obtain

$$\dot{E} = \dot{\boldsymbol{\theta}}^{\text{T}} \boldsymbol{Su} = Mg \tan \phi \dot{X}_g, \tag{15}$$

which specifies the relation between the robot's total mechanical energy and the X-position for CoM. Since this equation has redundant control inputs, we have to introduce another constraint. Let us then consider a solution yielded by the constant torque ratio, μ, which gives the condition of $u_1 = \mu u_2$. By substituting this into Eq. (15), the solution is
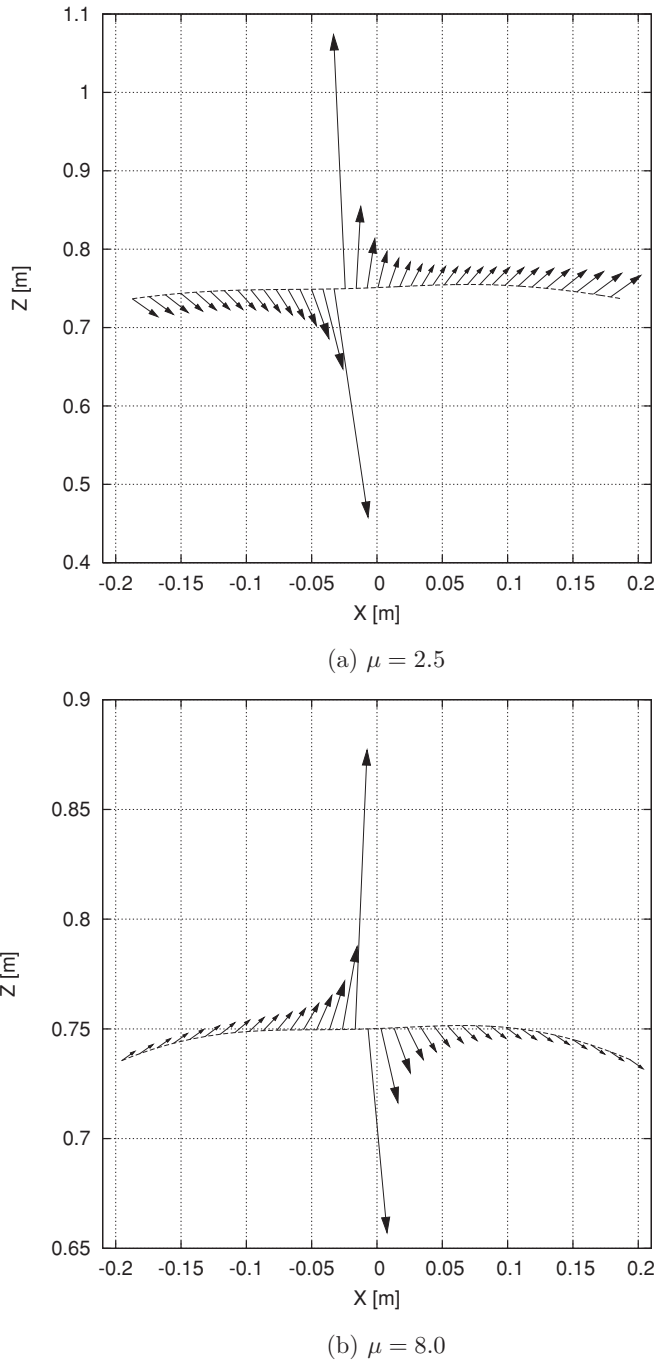
(a) $\mu = 2.5$

(b) $\mu = 8.0$

Fig. 3. Generalized virtual gravity vectors in VPDW with CTR formula.

determined as

$$
Su = \begin{bmatrix} \mu + 1 \\ -1 \end{bmatrix} \frac{Mg \tan \phi \dot{X}_g}{(\mu + 1)\dot{\theta}_1 - \dot{\theta}_2}. \tag{16}
$$

We call this the *CTR (constant torque ratio) formula*.[8] Note that this solution no longer has the meaning of uniform virtual gravity in the X-direction. The inverse transformation of this Su should yield the generalized virtual gravity vector.

3.2. Typical behaviors of generalized virtual gravity
Figure 3 plots the generalized virtual gravity vector along the CoM orbit with VPDW where $\phi = 0.02$ [rad]; $\mu = 2.5$

(Fig. 3(a)), (b) $\mu = 8.0$ (Fig. 3(b)). The robot's physical parameters were chosen as listed Table I. As can be seen from the results, the vectors are going to diverge as the system closes with the singular point of $\theta_1 = \theta_2$. As reported by Asano *et al.*,[8] the walking system's effectiveness where $\mu = 8.0$ is better or its walking speed is faster than that where $\mu = 2.5$. The results strongly indicate that generalized virtual gravity where $\mu = 8.0$ accelerates CoM more effectively than that where $\mu = 2.5$, and this supports the results of Asano *et al.*[8] As plotted in Fig. 3, the generalized virtual gravity of $\mu = 2.5$ has an unnecessary element perpendicular to $\dot{r}_g$ greater than that of $\mu = 8.0$, and this force element disrupts the forward acceleration of CoM as will be described later.

3.3. Analysis based on orthogonal projection on $\dot{r}_g$
The following relation is easily derived where $\theta_1 \neq \theta_2$.

$$
\dot{E} = \dot{\boldsymbol{\theta}}^{\mathrm{T}} Su = \dot{\boldsymbol{\theta}}^{\mathrm{T}} \boldsymbol{J}_g^{\mathrm{T}} \boldsymbol{J}_g^{-\mathrm{T}} Su = \dot{\boldsymbol{r}}_g^{\mathrm{T}} \boldsymbol{f}_g. \tag{17}
$$

Hence, Eq. (15) can be interpreted as a special case of Eq. (17) with the generalized virtual gravity vector in the form

$$
\boldsymbol{f}_g = \begin{bmatrix} Mg \tan \phi \\ 0 \end{bmatrix}. \tag{18}
$$

In other words, Eq. (17) is a two-dimensional case or a generalized case of Eq. (15). Let ${}^p \boldsymbol{f}_g$ be the orthogonal projection vector of $\boldsymbol{f}_g$ on $\dot{\boldsymbol{r}}_g$. Considering Eq. (17), this is given by

$$
{}^p \boldsymbol{f}_g = \frac{\dot{\boldsymbol{r}}_g^{\mathrm{T}} \boldsymbol{f}_g}{\dot{r}_g^2} \dot{\boldsymbol{r}}_g = \frac{\dot{E}}{\dot{r}_g^2} \dot{\boldsymbol{r}}_g, \tag{19}
$$

and can be divided into two parts, i.e., $\boldsymbol{f}_1$ due to the ankle-joint effect and $\boldsymbol{f}_2$ due to the hip-joint effect, as

$$
\begin{aligned}
{}^p \boldsymbol{f}_g &= \frac{\dot{\theta}_1 u_1 + (\dot{\theta}_1 - \dot{\theta}_2) u_2}{\dot{r}_g^2} \dot{\boldsymbol{r}}_g \\
&= \frac{\dot{\theta}_1 u_1}{\dot{r}_g} \frac{\dot{\boldsymbol{r}}_g}{\dot{r}_g} + \frac{(\dot{\theta}_1 - \dot{\theta}_2) u_2}{\dot{r}_g} \frac{\dot{\boldsymbol{r}}_g}{\dot{r}_g} \\
&=: {}^p \boldsymbol{f}_1 + {}^p \boldsymbol{f}_2. \tag{20}
\end{aligned}
$$

This projection enables us to avoid divergence at $\theta_1 = \theta_2$, and the generalized virtual gravity vector then becomes continuously visible unlike the results in Fig. 3. The norm ratio yields the power ratio as

$$
\frac{|{}^p \boldsymbol{f}_1|}{|{}^p \boldsymbol{f}_2|} = \frac{|\dot{\theta}_1 u_1|}{|(\dot{\theta}_1 - \dot{\theta}_2) u_2|}. \tag{21}
$$

We further define the coefficients of ${}^p \boldsymbol{f}_1$, ${}^p \boldsymbol{f}_2$, and ${}^p \boldsymbol{f}_g$ as

$$
{}^p f_1 := \frac{\dot{\theta}_1 u_1}{\dot{r}_g}, \quad {}^p f_2 := \frac{(\dot{\theta}_1 - \dot{\theta}_2) u_2}{\dot{r}_g}, \quad {}^p f_g := \frac{\dot{E}}{\dot{r}_g}. \tag{22}
$$

Figure 4 shows the time evolutions of ${}^p f_1$, ${}^p f_2$, and ${}^p f_g$ in VPDW with the CTR formula where $\mu = 2.5$ and 8.0.
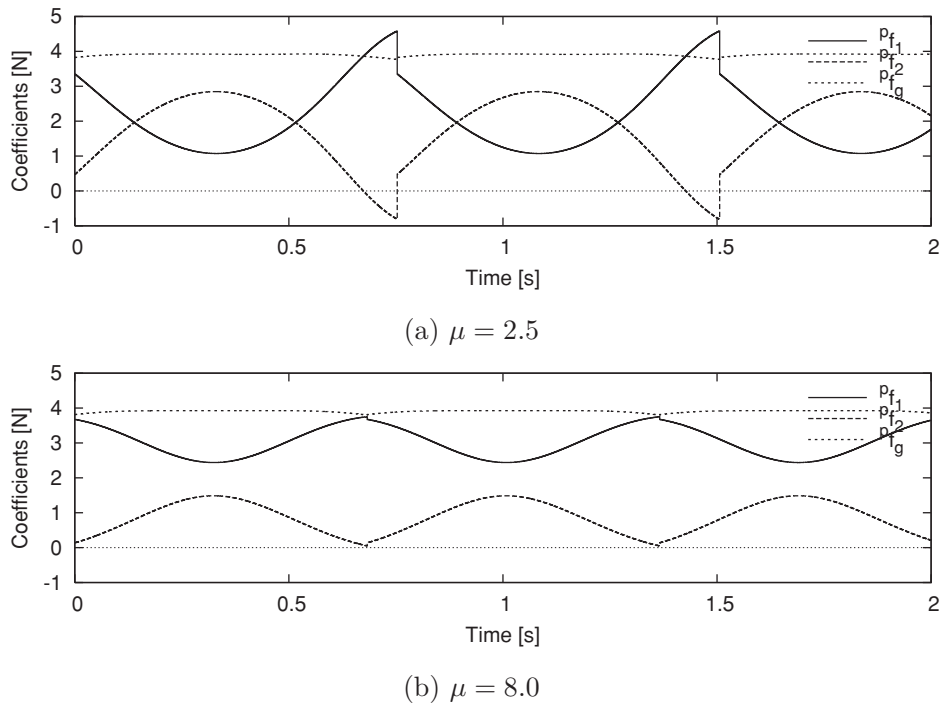
(a) $\mu = 2.5$

(b) $\mu = 8.0$

Fig. 4. Time evolutions of coefficients of orthogonal projective vectors $^p f_1$, $^p f_2$, and $^p f_g$.

Considering $\dot{X}_g > 0$ in the VPDW, the following inequality holds:

$$^p f_g = \frac{Mg \tan \phi \dot{X}_g}{\sqrt{\dot{X}_g^2 + \dot{Z}_g^2}} \leq \frac{Mg \tan \phi \dot{X}_g}{\dot{X}_g} = Mg \tan \phi. \quad (23)$$

The equality in Eq. (23) holds if $\dot{Z}_g$ is 0 or sufficiently small. In general, $^p f_g \approx Mg \tan \phi$ regardless of the system's chosen parameters as shown in Fig. 3 because the change of $\dot{Z}_g$ is sufficiently small. We therefore conclude that, regardless of μ, vector f_g has a magnitude of about $Mg \tan \phi$ in the $\dot{r}_g$-direction, and the reason the walking speed is decreased when μ is small cannot be explained by these results.

Let us now define the orthogonal vector of $^p f_g$ as

$$^p f_g^{\perp} := f_g - {}^p f_g, \quad (24)$$

and compare this magnitude with that of $^p f_g$. Note that $^p f_g^{\perp}$ does not contribute to restoring mechanical energy, i.e., $\dot{r}_g^{\mathrm{T}} {}^p f_g^{\perp} = 0$. Figure 5 shows the time evolutions of $|^p f_g^{\perp}|$,

where $\mu = 2.5$ and 8.0, and this clearly indicates that the magnitude where $\mu = 2.5$ is larger than that where $\mu = 8.0$. This means that the walking speed decrease when μ is small does not occur because it is impossible to drive CoM in the direction of $\dot{r}_g$ but because there is a large unnecessary force perpendicular to $\dot{r}_g$. Figure 6 shows the conditions for f_g and its projection vectors for small and large μ. The magnitudes of $^p f_g$ in both cases are almost equal to $Mg \tan \phi$, whereas those of $^p f_g^{\perp}$ are different. When μ is small, it is clear that $^p f_g^{\perp}$ increases gravity or drives the CoM downwards, which results in generating a counterclockwise torque around the foot contact point, and disrupts CoM from propelling forward to overcome the potential barrier at mid-stance.

4. Biped Model with Semicircular Feet and Underactuated Virtual Passive Dynamic Walking

Now that we have discussed the mechanism for the flat-feet model, let us investigate that for the semicircular-feet model in this section.
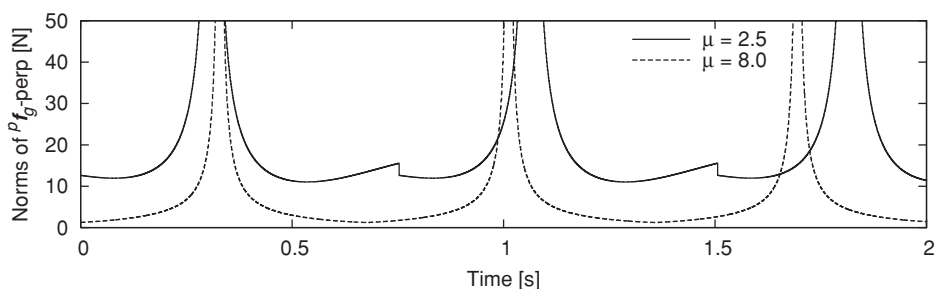

Fig. 5. Time evolution of norms of $^p f_g^{\perp}$ for $\mu = 2.5$ and 8.0 in VPDW with CTR formula.
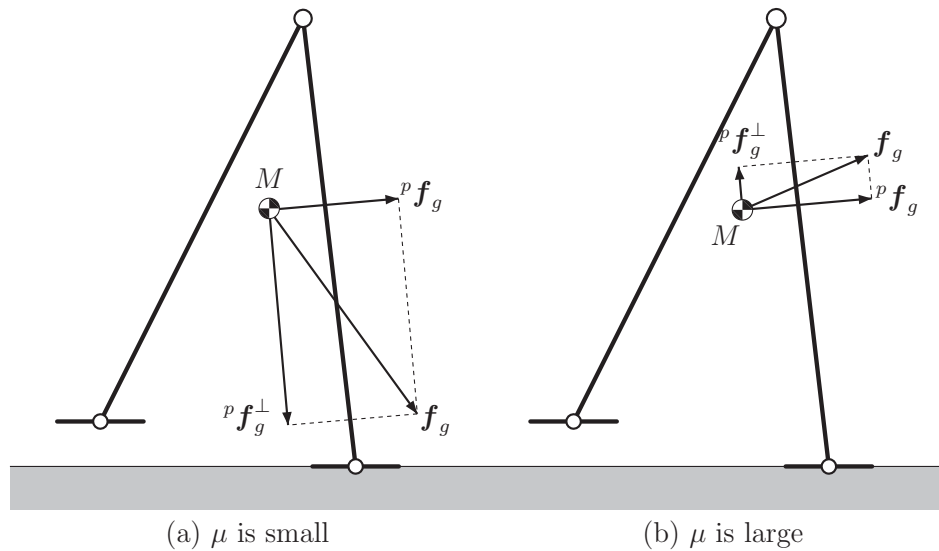
(a) μ is small   (b) μ is large

Fig. 6. Generalized virtual gravity conditions for small and large μ.
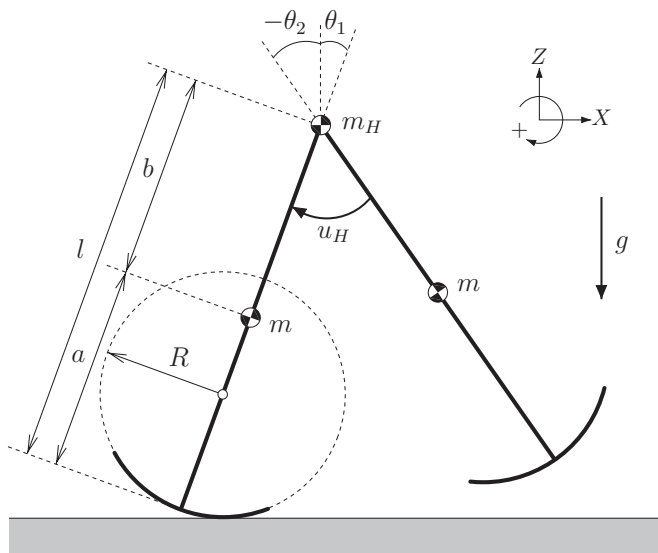

Fig. 7. Model of planar underactuated biped robot with semicircular feet.

4.1. Model with semicircular feet

In the following, we will consider the model shown in Fig. 7 whose foot mass is included in the leg mass. Let $\boldsymbol{\theta} = [\,\theta_1\ \theta_2\,]^{\mathrm{T}}$ be the generalized coordinate vector and u_H be the hip-joint torque. The dynamic equation for the robot is then given by

$$\boldsymbol{M}(\boldsymbol{\theta})\ddot{\boldsymbol{\theta}} + \boldsymbol{C}(\boldsymbol{\theta},\dot{\boldsymbol{\theta}})\dot{\boldsymbol{\theta}} + \boldsymbol{g}(\boldsymbol{\theta}) = \boldsymbol{S}u_H = \begin{bmatrix} 1 \\ -1 \end{bmatrix} u_H. \quad (25)$$

The details of the terms are as follows:

$$\boldsymbol{M}(\boldsymbol{\theta}) = \begin{bmatrix} M_{11} & M_{12} \\ M_{21} & M_{22} \end{bmatrix}, \quad \boldsymbol{C}(\boldsymbol{\theta},\dot{\boldsymbol{\theta}}) = \begin{bmatrix} C_{11} & C_{12} \\ C_{21} & 0 \end{bmatrix},$$

$$M_{11} = m\left(R^2 + (a-R)^2 + 2R(a-R)\cos\theta_1\right)$$
$$\qquad + (m_H + m)\left(R^2 + (l-R)^2 + 2R(l-R)\cos\theta_1\right),$$

$$M_{12} = M_{21} = -mb\left(R\cos\theta_2 + (l-R)\cos\theta_H\right),$$
$$M_{22} = mb^2,$$
$$C_{11} = -mR(a-R)\dot{\theta}_1\sin\theta_1 - (m_H + m)R(l-R)\dot{\theta}_1\sin\theta_1,$$
$$C_{12} = mb\dot{\theta}_2(R\sin\theta_2 - (l-R)\sin\theta_H),$$
$$C_{21} = mb(l-R)\dot{\theta}_1\sin\theta_H,$$
$$\boldsymbol{g}(\boldsymbol{\theta}) = \begin{bmatrix} -(m_H l + ml + ma - MR)\,g\sin\theta_1 \\ mbg\sin\theta_2 \end{bmatrix}.$$

We denote the hip-joint torque as u_H and as the relative hip-joint angle $\theta_H := \theta_1 - \theta_2$ to distinguish the underactuated model from the fully actuated one.

4.2. Underactuated virtual passive dynamic walking

The time derivative of mechanical energy in this case satisfies the relation $\dot{E} = \dot{\theta}_H u_H$. Virtual passive dynamic walking is then formulated as

$$\dot{E} = \dot{\theta}_H u_H = Mg\tan\phi\dot{X}_g, \quad (26)$$

and hip-joint torque u_H is uniquely determined as

$$u_H = \frac{Mg\tan\phi\dot{X}_g}{\dot{\theta}_H}. \quad (27)$$

We call the walking style driven only by the hip-joint torque of Eq. (27) *underactuated virtual passive dynamic walking (UVPDW)*. Equation (27) has singularity at $\dot{\theta}_H = 0$, but this does not matter because the system automatically avoids the singular point. Limit cycle walkers often exhibit *swing-leg retraction*,[9] which is the motion of the swing leg; it moves backward just prior to heel strike. UVPDW systems, however, do not exhibit this motion regardless of system parameter choices. See the Appendix for the detailed analysis. Figure 8 shows the simulation results for UVPDW where $R = 0.5$ [m] and $\phi = 0.01$ [rad]. Other system parameters where chosen as listed in Table I. We can see from Fig. 8(b) that condition $\dot{\theta}_1 > \dot{\theta}_2$ always holds,
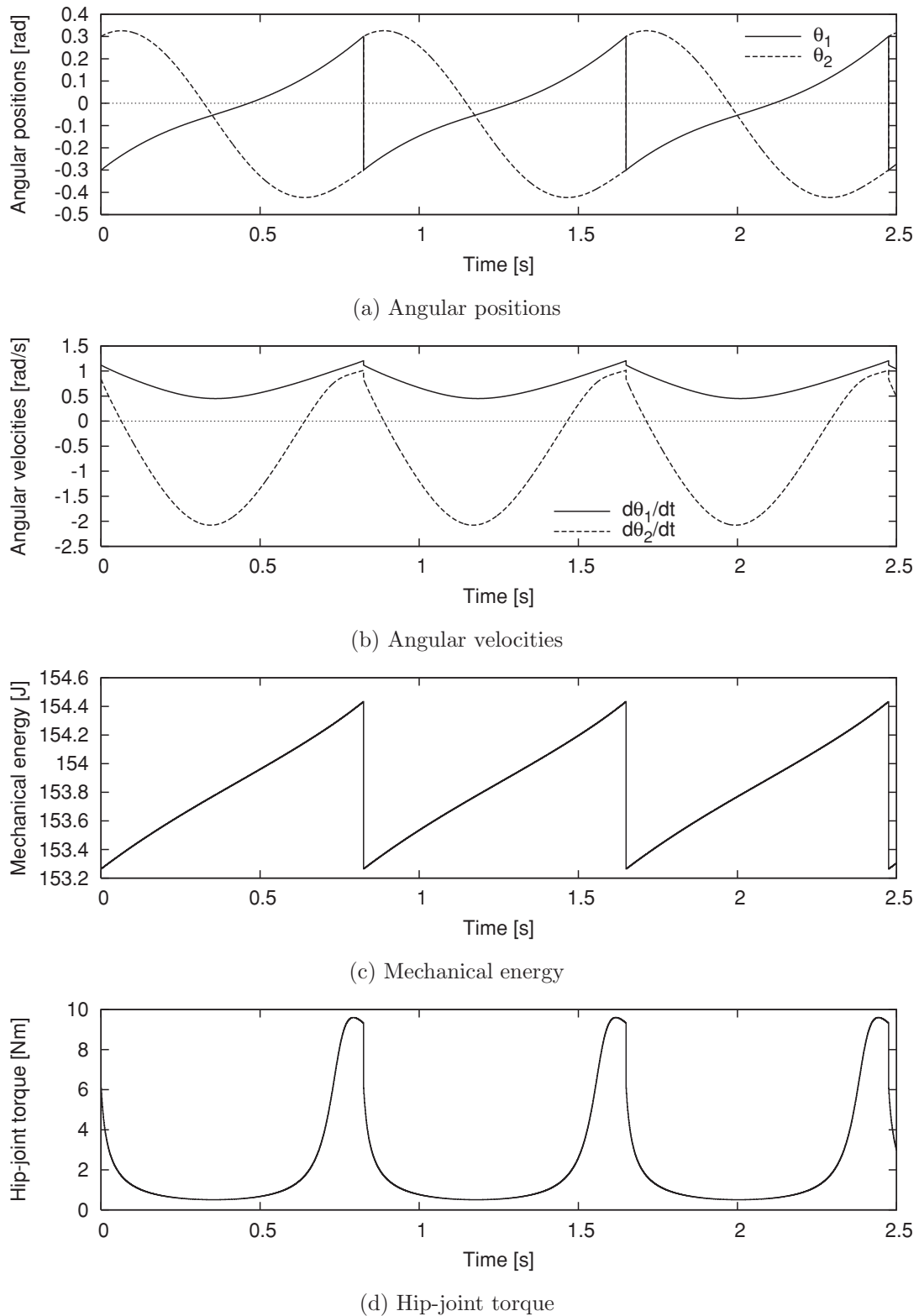
(a) Angular positions

(b) Angular velocities

(c) Mechanical energy

(d) Hip-joint torque

Fig. 8. Simulation results for underactuated VPDW with semicircular feet where $\phi = 0.01$ [rad].

and from (d) that control input u_H does not diverge during a cycle. Figure 9 has stick diagrams of UVPDW where (a) $\phi = 0.02$ and (b) $\phi = 0.03$ [rad]. Swing-leg retraction does not occur in either case and singularity is automatically avoided.

If condition $\dot{\theta}_H > 0$ holds, the maximum efficiency condition also holds. Energy efficiency is evaluated by specific resistance defined as

$$\text{specific resistance} = \frac{p}{Mgv}, \tag{28}$$

which means the energy consumption per distance traveled per kilogram mass per gravity. p is the consumed input power
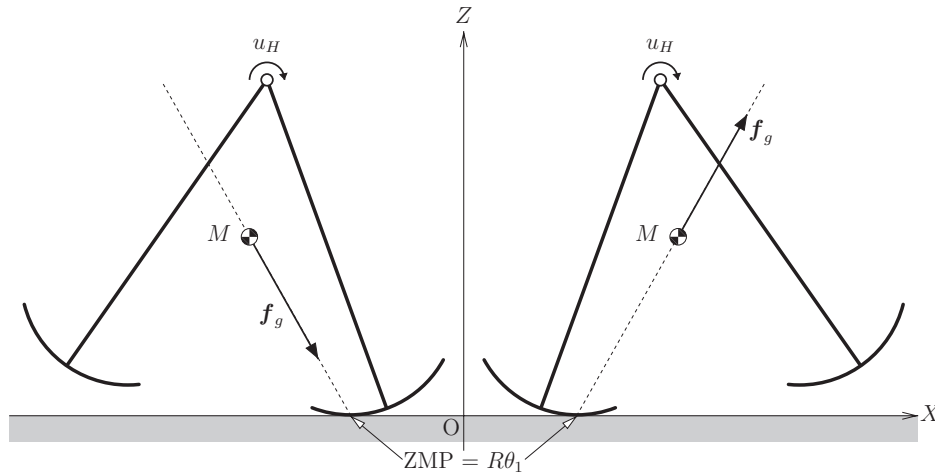
Fig. 9. Stick diagrams for underactuated VPDW with semicircular feet.

and v is the walking speed, and are defined as

$$p := \frac{1}{T} \int_{0^+}^{T^-} \left| \dot{\theta}_H u_H \right| \, \mathrm{d}t, \qquad (29)$$

$$v := \frac{1}{T} \int_{0^+}^{T^-} \dot{X}_g \, \mathrm{d}t = \frac{\Delta X_g}{T}. \qquad (30)$$

Using these equations, the maximum efficiency condition is derived as

$$\frac{p}{Mgv} = \frac{\int_{0^+}^{T^-} \left| \dot{\theta}_H u_H \right| \, \mathrm{d}t}{Mg \Delta X_g} \geq \frac{\int_{0^+}^{T^-} \dot{\theta}_H u_H \, \mathrm{d}t}{Mg \Delta X_g} = \frac{\Delta E}{Mg \Delta X_g}, \qquad (31)$$

where $\Delta E := E(T^-) - E(0^+)$. Because $\dot{\theta}_H > 0$ and $u_H > 0$, the equality in Eq. (31) holds and maximum efficiency is achieved. Since $\Delta E = Mg \tan \phi \Delta X_g$ holds in the case of VPDW, minimum specific resistance yields $\tan \phi$, and UVPDW always achieves this.

4.3. Generalized virtual gravity

Let the contact point of the sole with the ground when $\theta_1 = 0$ be the central point of the X–Z coordinate. Then, the general X-position of the contact point yields $R\theta_1$. The point in this model is equivalent to ZMP. The generalized virtual gravity vector of u_H yields

$$\boldsymbol{f}_g = \boldsymbol{J}_g(\boldsymbol{\theta})^{-\mathrm{T}} \begin{bmatrix} 1 \\ -1 \end{bmatrix} u_H = \frac{u_H}{\Delta_g} \left(\begin{bmatrix} R\theta_1 \\ 0 \end{bmatrix} - \boldsymbol{r}_g \right), \qquad (32)$$

and is found to be the vector from the contact point to the CoM. As shown in Fig. 10, it acts as centripetal force (left) or centrifugal (right).

Although there is *unreasonableness* that the robot must only be driven by central force during the cycle, the rolling effect overcomes this. The next section discusses our extensive investigations into finding the mechanism.
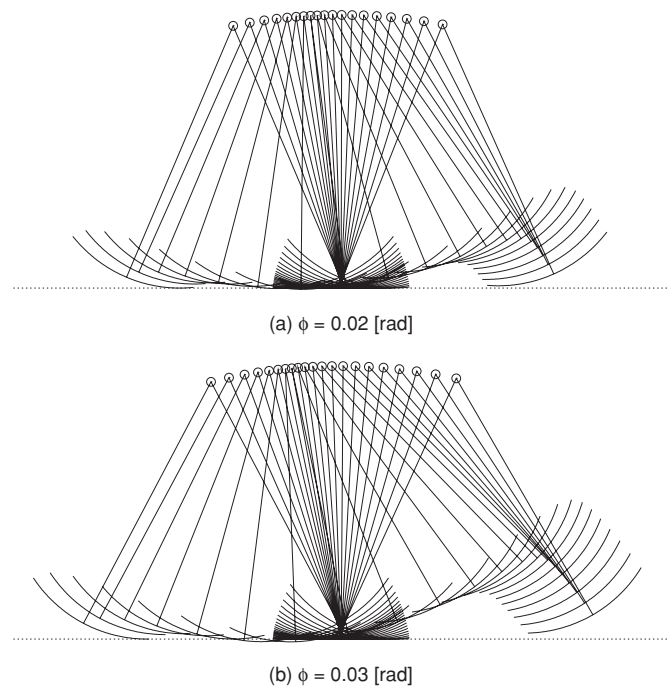

(a) $\phi = 0.02$ [rad]

(b) $\phi = 0.03$ [rad]

Fig. 10. Generalized virtual gravity in underactuated VPDW with semicircular feet.

5. Investigating Rolling Effect through Comparison with Virtual Flat-feet Model

This section investigates the rolling effect through linearization and compares the semicircular-feet model with the one for flat feet.

5.1. Linearization and comparison of two models

Linearizing the semicircular-feet model around the equilibrium point, $\boldsymbol{\theta} = \dot{\boldsymbol{\theta}} = \boldsymbol{0}_{2 \times 1}$, the inertia matrix yields

$$\boldsymbol{M}_0 = \begin{bmatrix} m_H l^2 + ma^2 + ml^2 & -mbl \\ -mbl & mb^2 \end{bmatrix}, \qquad (33)$$

and this does not have any terms concerning the foot radius, R. The linearization of the nonlinear vector, $\boldsymbol{C}\dot{\boldsymbol{\theta}}$, on the other
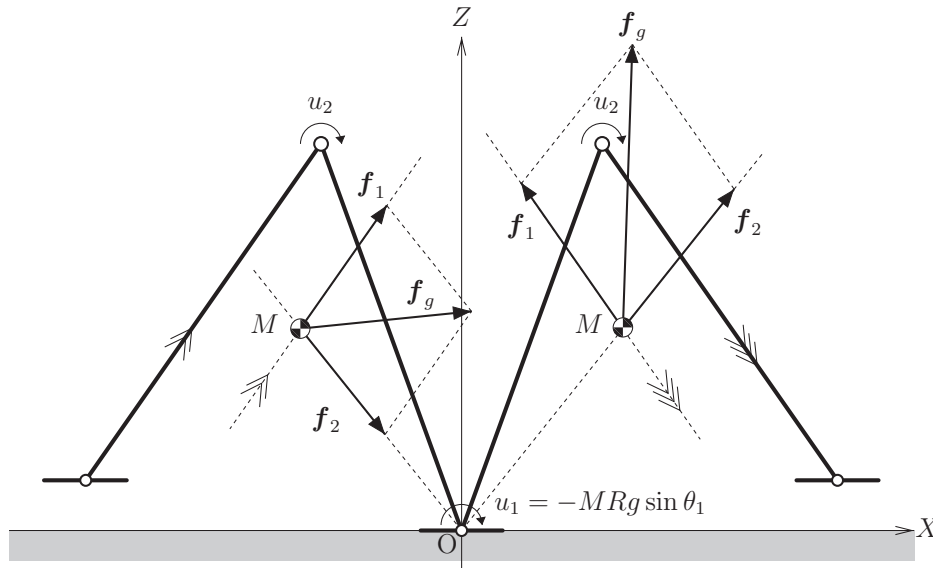
Fig. 11. Equivalent geometric relation of generalized virtual gravity vectors in Fig. 9.

hand, yields $\mathbf{0}_{2\times 1}$, and is equivalent to the flat-feet model's results. Matrix $\boldsymbol{M}$ and vector $\boldsymbol{C\dot\theta}$ of the two models are equivalent in the sense of a linearized system. Gravity term $\boldsymbol{g}(\boldsymbol{\theta})$ has differences. That of the semicircular-feet model can be divided into the following two terms:

$$\boldsymbol{g}(\boldsymbol{\theta}) = \begin{bmatrix} -(m_H l + ml + ma)\, g \sin\theta_1 \\ mbg \sin\theta_2 \end{bmatrix} + \begin{bmatrix} MRg \sin\theta_1 \\ 0 \end{bmatrix}. \tag{34}$$

The first term at the right-hand side is the same as the gravity term for the flat-feet model. The semicircular-feet model is therefore equivalent to that of the flat feet with ankle-joint torque, which is given as $-MRg \sin\theta_1$ in the context of a linearized system. The virtual ankle-joint torque accelerates CoM forward when $\theta_1 < 0$, whereas it decelerates in the case of $\theta_1 > 0$. Real hip-joint torque then effectively accelerates CoM forward together with virtual ankle-joint torque or the rolling effect. This driving mechanism is outlined in Fig. 11; the CoM of the virtual flat-feet model is properly accelerated forward by hip-joint torque reproducing virtual gravity effect and the virtual ankle-joint torque.

This can be explained from the angular momentum point of view. The time derivative of angular momentum, L, in the case of a free ankle joint, should satisfy $\dot{L} = MgX_g$. The effect of gravity then decreases the angular momentum when $X_g < 0$ and increases it when $X_g > 0$. The robot is accelerated automatically when $X_g > 0$ without any joint actuation after overcoming the potential barrier in this phase, the external driving force is not necessary. We thus need to exert some torque to drive CoM forward during the first half of the cycle to overcome the potential barrier at mid-stance.

Note that the change in mechanical energy change created by virtual ankle-joint torque is 0 because the following relation holds:

$$\int_{0^+}^{T^-} \dot\theta_1\,(-MRg \sin\theta_1)\,\mathrm{d}t = MRg \int_{0^+}^{T^-} \frac{\mathrm{d}\cos\theta_1}{\mathrm{d}t}\,\mathrm{d}t$$
$$= MRg\left(\cos\left(\theta_1(T^-)\right) - \cos\left(\theta_1(0^+)\right)\right) = 0. \tag{35}$$

Thus, the restoration of mechanical energy during the stance phase is only accomplished by *real* hip-joint torque. Note that we used relation $\theta_1(0^+) = -\theta_1(T^-)$ in the above calculation.

5.2. Typical gait of virtual flat-feet model

We conducted numerical simulations of UVPDW using a virtual flat-feet model with virtual ankle-joint torque to confirm these results. We used the nonlinear fully actuated flat-feet model of Eq. (1) with the hip-joint torque of Eq. (27) and the virtual ankle-joint torque of $-MRg \sin\theta_1$. Note that we used an inelastic collision model of heel strike not for the flat-feet model but that for semicircular feet because there is a major difference in the dissipation of mechanical energy. Semicircular feet decrease energy dissipation but this paper does not discuss the detailed mechanism responsible. See refs. [10, 11] for the detail. Figure 12 shows the simulation results. The conditions are the same as those in Fig. 8, and we can see that a similar gait is generated.

The total mechanical energy at $t = t_1$ ($0^+ \le t_1 \le T^-$) in Fig. 12(c) is virtually calculated by

$$E(t_1) = E(0^+) + \int_{0^+}^{t_1} \dot\theta_H u_H\,\mathrm{d}t, \tag{36}$$

taking only the power input by hip-joint torque into account. We can see that the mechanical energy produces the same orbit as normal VPDW. Figure 12(e) shows virtual ankle-joint torque, which changes from positive to negative; this leads us to conclude that virtual ZMP travels monotonically forward in the virtual sole.

(a) Angular positions

(b) Angular velocities

(c) Mechanical energy

(d) Hip-joint torque
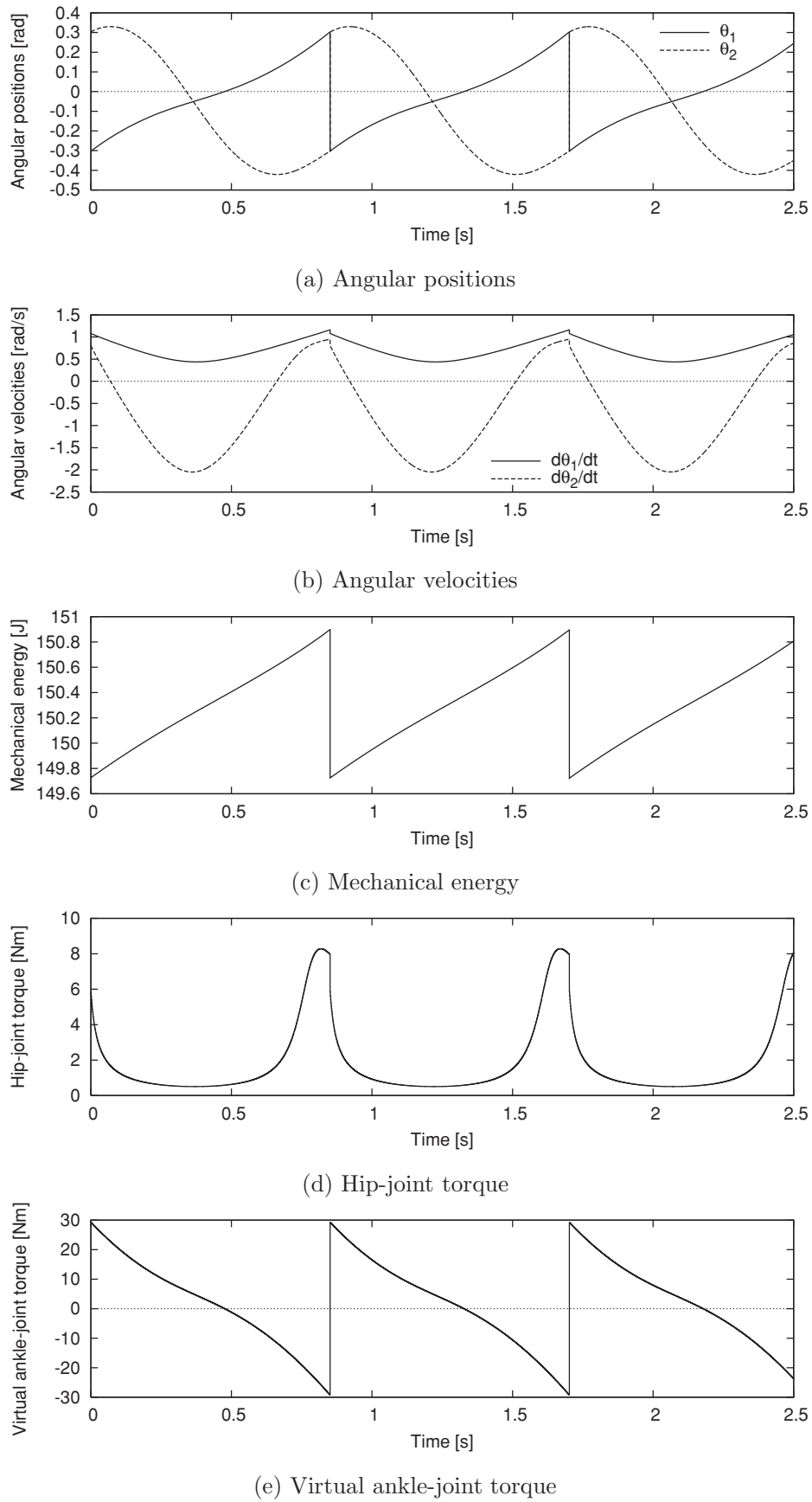

(e) Virtual ankle-joint torque

Fig. 12. Simulation results for equivalent underactuated VPDW of virtual flat-feet model where $\phi = 0.01$ [rad].
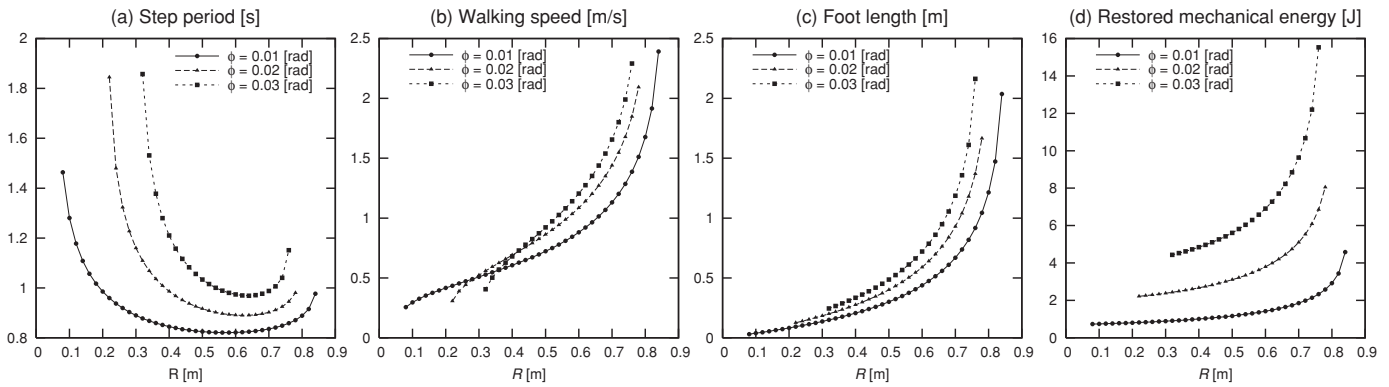
Fig. 13. Gait descriptors of underactuated VPDW for three values of ϕ with respect to foot radius R.

5.3. Effect of foot radius on walking speed
The X-position at CoM is given by

$$X_g = R(\theta_1 - \sin \theta_1)$$
$$+ \frac{(m_H l + ma + ml) \sin \theta_1 - mb \sin \theta_2}{M}, \quad (37)$$

and its time derivative yields

$$\dot{X}_g = R\dot{\theta}_1(1 - \cos \theta_1)$$
$$+ \frac{(m_H l + ma + ml)\dot{\theta}_1 \cos \theta_1 - mb\dot{\theta}_2 \cos \theta_2}{M}. \quad (38)$$

Note that $\cos \theta_1 \approx 1$ when θ_1 is sufficiently small and thus the first term at the right-hand side of Eq. (38) is almost 0. We then find $\dot{X}_g$ is not directly affected by R. Although foot radius R appears as virtual ankle-joint torque to drive CoM, it does not increase the CoM velocity, $\dot{X}_g$, directly. As shown by Asano and Luo,[10, 11] the reason semicircular feet increase the walking speed lies in the heel-strike mechanism. It should be noticed that the rolling effect contributes to overcome the potential barrier, but does not increase the walking speed.

Here, we briefly describe the effect of semicircular feet on mechanical energy dissipation caused by heel strikes. Let $\dot{\theta}^- \in \mathbb{R}^2$ be the angular velocity vector just before impact, then the dissipated mechanical energy is given by

$$\Delta E_{\mathrm{hs}} = -\frac{1}{2}(\dot{\theta}^-)^{\mathrm{T}} N \dot{\theta}^- \le 0, \quad (39)$$

where matrix $N \in \mathbb{R}^{2 \times 2}$ is positive semidefinite and a function of the angular positions and physical parameters including the foot radius. Through analysis based on singular value of matrix N, we found that there was a tendency for mechanical energy dissipation to decrease with the increase in foot radius.[10] If $R < l$, mechanical energy dissipation always occurs. Where $R = l$, however, the dissipated mechanical energy yields

$$\Delta E_{\mathrm{hs}} = -\frac{\sigma_1}{4}(\dot{\theta}_H^-)^2, \quad (40)$$

where σ_1 is the maximum singular value of matrix N. We can conclude that the mechanical energy dissipation caused by

heel strikes can be reduced to zero by achieving $\dot{\theta}_H^- = 0$ regardless of the choice of physical parameters for the walking system. These results supports McGeer's original study on a synthetic wheel.[1]

We can summarize the effects semicircular feet had on dynamic bipedal walking as follows:

■ Semicircular feet provide a rolling effect that is equivalent to ankle-joint torque during the stance phase.
■ Semicircular feet reduce the dissipation of mechanical energy at the instant of inelastic heel-strike collisions.

6. Parameter Study
This section discusses our analysis of changes in gait according to the foot radius and mass ratio.

6.1. Effect of foot radius
Let us first examine the effect of the foot radius, R. Figure 13 shows the analysis results of the gait descriptors for three values of ϕ. Here, Fig. 13(a) shows the step period, Fig. 13(b) the walking speed, Fig. 13(c) the specific resistance, and Fig. 13(d) the restored mechanical energy. We can see that the walking speed and specific resistance monotonically improve with the increase in R. This is because the rolling effect of larger foot radius causes excessive acceleration of CoM. With large foot radius, as seen in Fig 13(d), there is a great deal of acceleration and consequently much mechanical energy is restored. In addition, it is also seen that larger ϕ provides faster gait.

Next, the nominal leg-mass position, a, or the length from the tiptoe to CoM, is chosen as three values while maintaining $a + b = l = 1.0$ [m]. Figure 14 shows the analysis results of the gait descriptors where $\phi = 0.02$ [rad]. For all a, the descriptors show almost the same tendency with the increase in R as the above result. It should be remarked that, as seen in the results, small R has less effect in propelling the walking robot forward, and the stable gait cannot be generated. If $R = 0$ or without semicircular feet nor ankle-joint actuation, so-called *stilt-type* walkers,[12] are thus disadvantageous in generating a high-speed gait. The related results are reported in Asano *et al.*[8]

Large R virtually provides large ankle-joint torque and has shock-absorbing effect for impact as previously mentioned. The walking speeds thus obtained are remarkably faster than
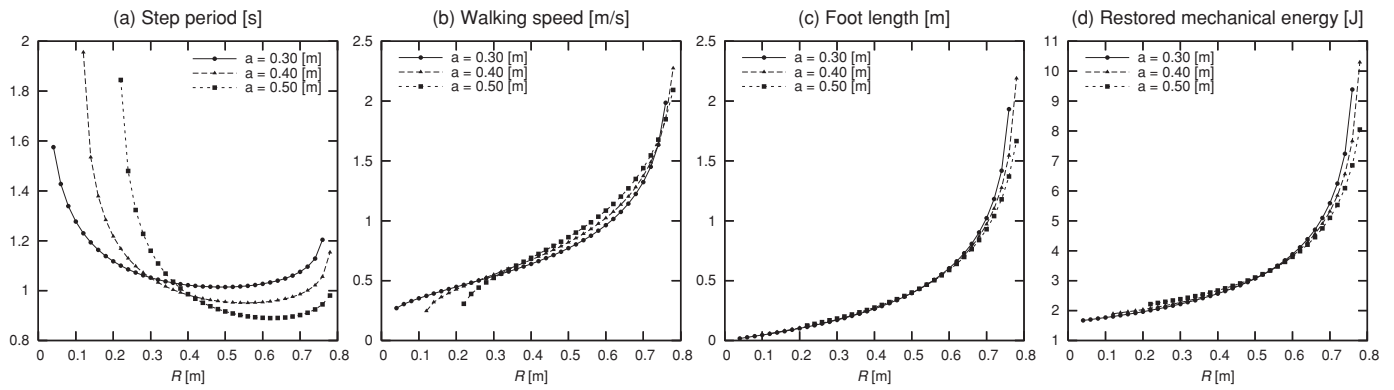
Fig. 14. Gait descriptors of underactuated VPDW for three values of a with respect to foot radius R where $\phi = 0.02$ [rad].

those with previous major approaches inspired by passive dynamic walking with ankle-joint actuation using flat footed models.[3, 8] If R is chosen as too large, however, the gait diverges due to the excessive acceleration.

6.2. Effect of mass ratio

McGeer studied dynamics of a synthetic wheel that is a compass-like biped robot with semicircular feet and a large point mass at the hip, and pointed out that the robot can also walk on level ground without energy supply if $R = l$ and $m_H \gg m$. As mentioned above, however, R cannot be chosen as so large because the steady motion is disturbed. We now investigate the effect of mass ratio of hip mass to leg mass on the gait efficiency. Let us define $\gamma := m_H / m$ [-] and analyze the gait descriptors. Figure 15 shows the analysis results for three values of ϕ. We can see that the gait efficiency, walking speed, and specific resistance, monotonically worsen with the increase in γ. This is because hip-joint actuation cannot cause restoration of mechanical energy by actuating massless swing-leg.

Considering these results, we must conclude that it is hard to reproduce the motion as a synthetic wheel by realistic dynamic walkers. In addition, we can state that dynamic walkers with massless legs, such as the simplest walking model,[13] always need to ankle-joint actuation. Synthetic wheel is an ideal model and is available only in the case without actuation nor external energy supply.

7. Conclusion and Future Work

This paper investigated the mechanisms of planar compass-like biped robots with flat or semicircular feet based on the concept of a generalized virtual gravity. The relation of a flat-feet model between CoM and joint torque was first investigated and the importance of ankle-joint torque was theoretically clarified. It was numerically shown that UVPDW can be accomplished in the case with semicircular feet, and the relation between the rolling effect and the ankle-joint torque was clarified.

Second, a virtual flat-feet model was introduced and its feasibility was evaluated. The authors believe that walkers with semicircular feet should be treated not as the "synthetic wheel" McGeer considered but as a virtual fully actuated system whose ankle-joint torque is uniquely determined by the foot radius R, the robot's total mass M, and the stance-leg angle θ_1. This further implies that the optimal convex curve for feet can be designed if the optimal ankle-joint torque is determined. Further investigations are therefore necessary.

Optimizing the convex curve of the foot is a subject left for future work. The mechanism responsible for increasing the stable domain of limit cycles is also a critical problem that needs to be theoretically clarified.

There has been a tendency to adopt flat feet in conventional biped humanoid robot design. A semicircular foot attached to the stance leg, however, virtually functions as ankle-joint torque during the stance phase and as a shock absorber in heel
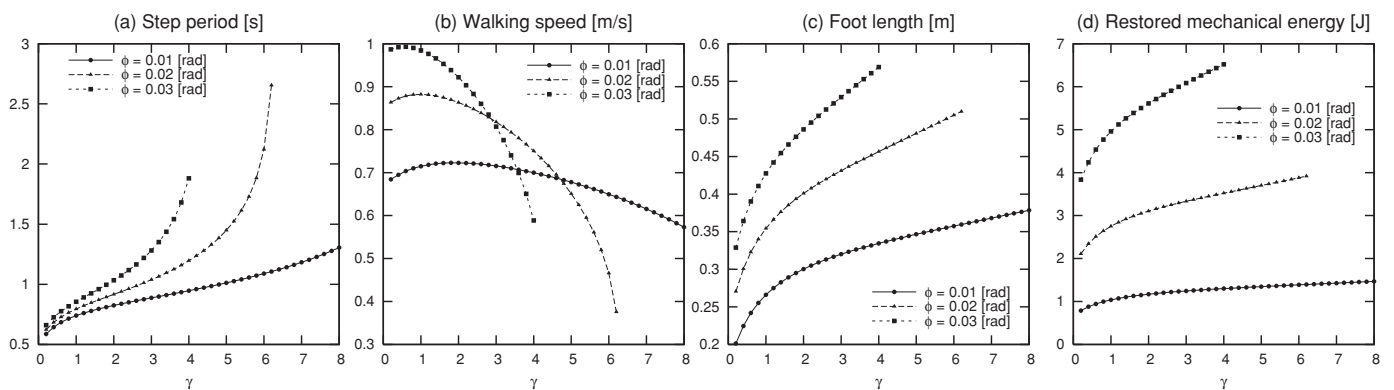

Fig. 15. Gait descriptors of underactuated VPDW for three values of ϕ with respect to mass ratio γ.

(a) Angular positions
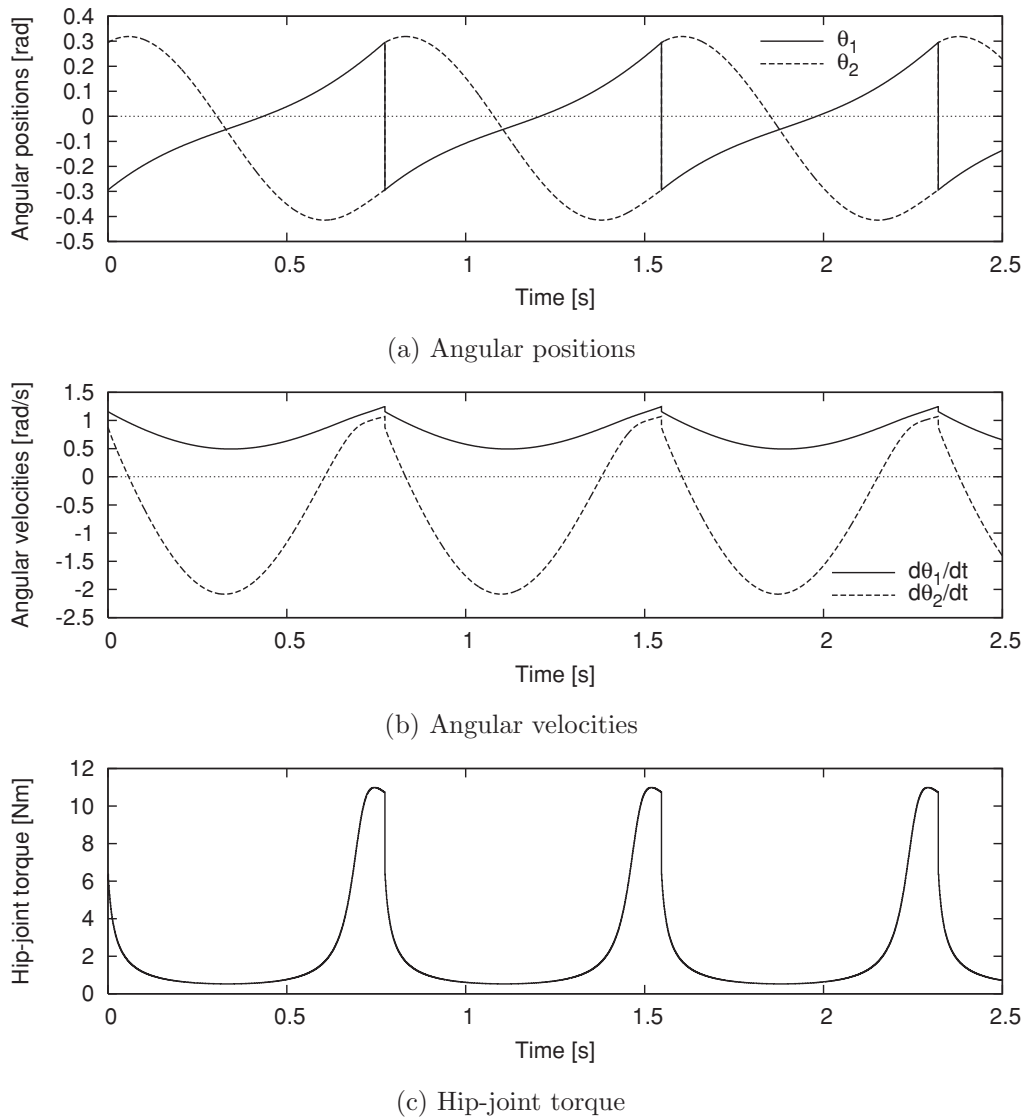

(b) Angular velocities

(c) Hip-joint torque

Fig. 16. Simulation results for linearized underactuated VPDW where $\phi = 0.01$ [rad].

strikes. The walking system's efficiency was improved as a result and the difficulties arising from the ZMP constraint were also eliminated. This suggests that it is necessary to reconsider the biped-robot mechanism with flat feet or the ZMP-based approach.

Appendix: On automatic singularity avoidance
In this Appendix, we outline the proof of automatic singularity avoidance. The phenomenon $\dot{\theta}_H = 0$ can be mathematically explained via linearization of the walking system.

The linearized model of Eq. (25) around the equilibrium point $\boldsymbol{\theta} = \mathbf{0}_{2\times 1}$ and $\dot{\boldsymbol{\theta}} = \mathbf{0}_{2\times 1}$ is given by

$$\boldsymbol{M}_0\ddot{\boldsymbol{\theta}} + \boldsymbol{G}_0\boldsymbol{\theta} = \boldsymbol{S}u_H, \qquad (41)$$

where matrix $\boldsymbol{M}_0$ is the same as in Eq. (33), and matrix $\boldsymbol{G}_0$ is given by

$$\boldsymbol{G}_0 = \begin{bmatrix} -(m_H l + ma + ml - MR)g & 0 \\ 0 & mbg \end{bmatrix}. \qquad (42)$$

Here we introduce a new coordinate $\bar{\boldsymbol{\theta}} := [\,\theta_1\ \theta_H\,]^{\mathrm{T}}$ to discuss the dynamics more clearly. The following relation,

$$\boldsymbol{\theta} = \boldsymbol{T}\bar{\boldsymbol{\theta}}, \quad \boldsymbol{T} = \begin{bmatrix} 1 & 0 \\ 1 & -1 \end{bmatrix}, \qquad (43)$$
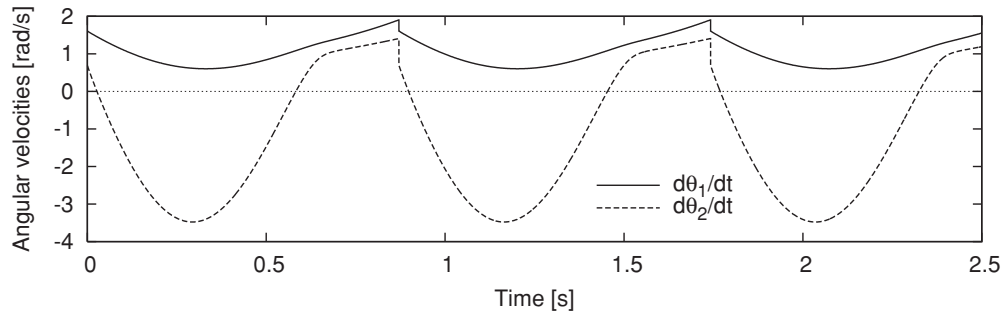
Fig. 17. Time evolution of angular velocities in linearized underactuated VPDW where $\phi = 0.03$ [rad].

holds and by multiplying both sides of Eq. (41) by $\boldsymbol{T}^{\mathrm{T}}$ from left-hand side, we obtain

$$\boldsymbol{T}^{\mathrm{T}}\boldsymbol{M}_0\boldsymbol{T}\ddot{\bar{\boldsymbol{\theta}}} + \boldsymbol{T}^{\mathrm{T}}\boldsymbol{G}_0\boldsymbol{T}\bar{\boldsymbol{\theta}} = \boldsymbol{T}^{\mathrm{T}}\boldsymbol{S}u_H = \begin{bmatrix} 0 \\ 1 \end{bmatrix} u_H. \quad (44)$$

We denote this as

$$\bar{\boldsymbol{M}}_0\ddot{\bar{\boldsymbol{\theta}}} + \bar{\boldsymbol{G}}_0\bar{\boldsymbol{\theta}} = \begin{bmatrix} 0 \\ 1 \end{bmatrix} u_H. \quad (45)$$

We further arrange this as the following canonical form:

$$\frac{\mathrm{d}}{\mathrm{d}t}\begin{bmatrix} \bar{\boldsymbol{\theta}} \\ \dot{\bar{\boldsymbol{\theta}}} \end{bmatrix} = \begin{bmatrix} \boldsymbol{0}_{2\times2} & \boldsymbol{I}_2 \\ -\bar{\boldsymbol{M}}_0^{-1}\bar{\boldsymbol{G}}_0 & \boldsymbol{0}_{2\times2} \end{bmatrix}\begin{bmatrix} \bar{\boldsymbol{\theta}} \\ \dot{\bar{\boldsymbol{\theta}}} \end{bmatrix} + \begin{bmatrix} \boldsymbol{0}_{2\times1} \\ \bar{\boldsymbol{M}}_0^{-1}\begin{bmatrix} 0 \\ 1 \end{bmatrix} \end{bmatrix} u_H. \quad (46)$$

This has a form of a linear system with a nonlinear feedback of u_H.

In calculating u_H, we also linearized X_g in Eq. (37) as

$$\bar{X}_g = \frac{(m_H l + 2ma)\theta_1 + mb\theta_H}{M}, \quad (47)$$

and used its time-derivative

$$\dot{\bar{X}}_g = \frac{(m_H l + 2ma)\dot{\theta}_1 + mb\dot{\theta}_H}{M}$$
$$= \begin{bmatrix} (m_H l + 2ma)/M & mb/M \end{bmatrix} \cdot \begin{bmatrix} \dot{\theta}_1 \\ \dot{\theta}_H \end{bmatrix} =: \bar{\boldsymbol{J}}_X\dot{\bar{\boldsymbol{\theta}}}. \quad (48)$$

Figure 16 shows the simulation results of linearized UVPDW where $\phi = 0.01$ [rad]. Note that, however, we applied the collision model of original nonlinear model with semicircular feet. The physical parameters were chosen as Table I. Compared the results of Fig. 8 with those of 12, we can see that the walking motion is almost the same. $\dot{\theta}_2$ once approaches to $\dot{\theta}_1$ but then it repels. This result suggests that the phenomenon comes not from the nonlinearity of dynamic equation but from the peculiarity of the control input, u_H. To confirm the phenomenon close to the singularity, we further

conducted numerical simulation where $\phi = 0.03$ [rad], and Fig. 17 shows the result of time evolution of the angular velocities. The result strongly indicate the phenomenon.

Using Eq. (48), the linearized control input is given by

$$u_H = \frac{Mg\tan\phi}{\dot{\theta}_H}\bar{\boldsymbol{J}}_X\dot{\bar{\boldsymbol{\theta}}}, \quad (49)$$

and the system of Eq. (46) can then be arranged as

$$\frac{\mathrm{d}}{\mathrm{d}t}\begin{bmatrix} \bar{\boldsymbol{\theta}} \\ \dot{\bar{\boldsymbol{\theta}}} \end{bmatrix} = \boldsymbol{A}\begin{bmatrix} \bar{\boldsymbol{\theta}} \\ \dot{\bar{\boldsymbol{\theta}}} \end{bmatrix}$$
$$:= \begin{bmatrix} \boldsymbol{0}_{2\times2} & \boldsymbol{I}_2 \\ -\bar{\boldsymbol{M}}_0^{-1}\bar{\boldsymbol{G}}_0 & \frac{Mg\tan\phi}{\dot{\theta}_H}\bar{\boldsymbol{M}}_0^{-1}\begin{bmatrix} 0 \\ 1 \end{bmatrix}\bar{\boldsymbol{J}}_X \end{bmatrix}$$
$$\times \begin{bmatrix} \bar{\boldsymbol{\theta}} \\ \dot{\bar{\boldsymbol{\theta}}} \end{bmatrix}. \quad (50)$$

Matrix $\boldsymbol{A} \in \mathbb{R}^{4\times4}$, however, is not constant and includes the singularity. By extracting the fourth row of Eq. (50) and substituting the values of Table I, we get

$$\ddot{\theta}_H = f_H(\boldsymbol{\theta}) + 1.31\frac{\dot{\theta}_1}{\dot{\theta}_H}, \quad (51)$$

$$f_H(\boldsymbol{\theta}) = 17.4\theta_1 - 24.0\theta_H + 0.218. \quad (52)$$

The function $f_H(\boldsymbol{\theta})$ is positive in the posture of Fig. 7. The second term of the right-hand side in Eq. (51) is positive at first because $\dot{\theta}_1$ is always positive during the stance phase, and $\dot{\theta}_H$ is also positive during swinging the swing leg forward. In passive or semipassive gaits, however, $\dot{\theta}_H$ often becomes negative just prior to impact. In other words, swing-leg retraction occurs. In UVPDW, as $\dot{\theta}_H \to 0$, $\ddot{\theta}_H$ increases and thus repels the singular point.

References
1. T. McGeer, "Passive dynamic walking," *Int. J. Robot. Res.* **9**(2), 62–82 (Apr. 1990).
2. M. Vukobratović and J. Stepanenko, "On the stability of anthropomorphic systems," *Math. Biosci.* **15**, 1–37 (Oct. 1972).
3. A. Goswami, B. Espiau and A. Keramane, "Limit cycles in a passive compass gait biped and passivity-mimicking control laws," *Auton. Robot.* **4**(3), 273–286 (Sep. 1997).

4. F. Asano and M. Yamakita, "Virtual gravity and coupling control for robotic gait synthesis," *IEEE Trans. Syst., Man Cybern. Part A: Syst. Humans* **31**(6), 737–745 (Nov. 2001).
5. S. Collins, A. Ruina, R. Tedrake and M. Wisse, "Efficient bipedal robots based on passive-dynamic walkers," *Sci. Mag.* **307**(5712), 1082–1085 (Feb. 2005).
6. R. Tedrake, T. W. Zhang, M. Fong and H. S. Seung, "Actuating a simple 3D passive dynamic walker," *Proceedings of the IEEE International Conferance on Robotics and Automation*, New Orleans, LA, USA (Apr. 2004) pp. 4656–4661.
7. M. Wisse, A. L. Schwab, R. Q. van der Linde and F. C. T. van der Helm, "How to keep from falling forward: Elementary swing leg action for passive dynamic walkers," *IEEE Trans. Robot.* **21**(3), 393–401 (Jun. 2005).
8. F. Asano, Z.-W. Luo and M. Yamakita, "Biped gait generation and control based on a unified property of passive dynamic walking," *IEEE Trans. Robot.* **21**(4), 754–762 (Aug. 2005).
9. A. Seyfarth, H. Geyer and H. Herr, "Swing-leg retraction: A simple control model for stable running," *J. Exp. Bio.* **206**(15), 2547–2555 (Aug. 2003).
10. F. Asano and Z.-W. Luo, "The effect of semicircular feet on energy dissipation by heel-strike in dynamic biped locomotion," *Proceedings of the IEEE International Conferance on Robotics and Automation*, Roma, Italy (Apr. 2007) pp. 3976–3981.
11. F. Asano and Z.-W. Luo, "Energy-efficient and high-speed dynamic biped locomotion based on principle of parametric excitation," *IEEE Trans. Robot.* **24**(6), 1289–1301 (Dec. 2008).
12. H. Miura and I. Shimoyama, "Dynamic walk of a biped," *Int. J. Robot. Res.* **3**(2), 60–74 (Jun. 1984).
13. M. Garcia, A. Chatterjee, A. Riuna and M. Coleman, "The simplest walking model: stability, complexity and scaling," *ASME J. Biomech. Eng.* **120**(2), 281–288 (Apr. 1998).